Acta Pharmacologica Sinica

www.nature.com/aps

ARTICLE

Pyk2 inhibition attenuates hypoxic-ischemic brain injury in neonatal mice

Jie Zhu[1], Shi-feng Chu[1], Ye Peng[1,2], Dan-dan Liu[1], Chen Chen[1], Wen-xuan Jian[1,3], Hong-shuo Sun[4], Zhong-ping Feng[4], Zhao Zhang[1] and Nai-hong Chen[1,2,3]

Newborns suffering from hypoxia-ischemia (HI) brain injury still lack effective treatment. Proline-rich tyrosine kinase 2 (Pyk2) is a non-receptor tyrosine kinase, which is highly correlated with transient ischemic brain injury in adult. In this study, we investigated the role of Pyk2 in neonatal HI brain injury. HI was induced in postnatal day 7 mouse pups by unilateral common carotid artery ligation followed by hypoxic exposure. Pyk2 interference lentivirus (LV-Pyk2 shRNA) was constructed and injected into unilateral cerebral ventricle of neonatal mice before HI. Infarct volume, pathological changes, and neurological behaviors were assessed on postnatal day 8–14. We showed that the phosphorylation level of Pyk2 was significantly increased in neonatal brain after HI, whereas LV-Pyk2 shRNA injection significantly attenuated acute HI brain damage and improved neurobehavioral outcomes. In oxygen-glucose deprivation-treated cultured cortical neurons, Pyk2 inhibition significantly alleviated NMDA receptor-mediated excitotoxicity; similar results were also observed in neonatal HI brain injury. We demonstrated that Pyk2 inhibition contributes to the long-term cerebrovascular recovery assessed by laser speckle contrast imaging, but cognitive function was not obviously improved as evaluated in Morris water maze and novel object recognition tests. Thus, we constructed lentiviral LV-HIF-Pyk2 shRNA, through which HIF-1α promoter-mediated interference of Pyk2 would occur during the anoxic environment. Intracerebroventricular injection of LV-HIF-Pyk2 shRNA significantly improved long-term recovery of cognitive function in HI-treated neonatal mice. In conclusion, this study demonstrates that Pyk2 interference protects neonatal brain from hypoxic-ischemic injury. HIF-1α promoter-mediated hypoxia conditional control is a useful tool to distinguish between hypoxic period and normal period. Pyk2 is a promising drug target for potential treatment of neonatal HI brain injury.

Keywords: neonatal mice; hypoxic-ischemic brain injury; Pyk2; NMDA receptor; excitotoxicity; HIF-1α

Acta Pharmacologica Sinica (2022) 43:797–810; https://doi.org/10.1038/s41401-021-00694-5

INTRODUCTION

Neonatal hypoxic-ischemic brain injury is the main cause of hypoxic-ischemic encephalopathy (HIE), which is a group of neurological disabilities in neonates characterized by neurodevelopmental delay, mental retardation, cerebral palsy, cognitive and motor impairments, and epilepsy and seizure disorders. Clinically, there is no effective therapy or treatment for hypoxic-ischemic (HI) brain injury and associated HIE. Supportive care and mild hypothermia are currently the only clinical management strategies for HI brain injury and related brain disorders [1]. Despite the availability of hypothermia therapy, the incidence of HI brain injury still ranges from 1 to 8 per 1000 live births in developed countries and 26 per 1000 live births in underdeveloped countries [2, 3]. Among surviving newborns, more than one million develop severe and chronic neuropsychological impairments, including cerebral palsy, epilepsy, and motor and cognitive deficits. Therefore, the development of effective neuroprotective agents for HI remains an important goal for medical research.

The onset cycle of HI can be divided into three stages: the first stage involves depolarization of neurons caused by hypoxia-ischemia. Excitotoxic injury is caused by excessive release of neurotransmitters mediated by calcium ion influx. The second stage involves oxidative stress caused by mitochondrial dysfunction and reactive oxygen species (ROS) release, which aggravates neuronal death. The third stage features an increase in the expression of inflammatory factors caused by changes in the brain environment, which leads to a higher risk of neuronal death [4]. Therefore, the treatment of this disease should be focused on saving neurons from neuronal excitotoxic injury early after HI injury, thus reducing the ischemic core area [5]. *N*-methyl-*D*-aspartate (NMDA) receptor-mediated excitotoxicity is the main mechanism by which cerebral ischemia causes damage. However, NMDA receptor antagonists are not clinically effective against stroke [6] or neonatal HI brain injury [7]. Blockade of NMDA receptors during late fetal or early neonatal life triggers widespread apoptotic neurodegeneration in the developing rat brain. The NMDA receptor downstream signaling protein postsynaptic

[1]State Key Laboratory of Bioactive Substances and Functions of Natural Medicines, Institute of Materia Medica & Neuroscience Center, Chinese Academy of Medical Sciences and Peking Union Medical College, Beijing 100050, China; [2]College of Pharmacy, Hunan University of Chinese Medicine, Changsha 410208, China; [3]Institute of Clinical Pharmacology, Guangzhou University of Chinese Medicine, Guangzhou 510720, China and [4]Department of Physiology, Faculty of Medicine, University of Toronto, Toronto, ON, Canada
Correspondence: Zhao Zhang (zhangzhao@imm.ac.cn) or Nai-hong Chen (chennh@imm.ac.cn)

Received: 3 January 2021 Accepted: 7 May 2021
Published online: 5 July 2021

density 95 (PSD95), a scaffolding protein involved in clustering glutamate receptors together with other proteins at postsynaptic sites, has been identified as a target in cerebral ischemia.

Proline-rich tyrosine kinase 2 (Pyk2) is a non-receptor tyrosine kinase that belongs to the focal adhesion kinase (FAK) family. Pyk2 expression is highly correlated with transient ischemic brain injury in adults [8]. PSD95 mediates the interaction between Pyk2 and NMDA receptors. Lithium-induced inhibition of Pyk2 Tyr-402 phosphorylation and the interaction of phosphorylated Pyk2 with PSD95 and NR2A ultimately leads to the inhibition of NMDA receptor-mediated excitotoxicity [9]. However, neonatal HI is not the same as adult HI, mainly due to differences in metabolism and NMDA receptor expression between the adult and neonatal brains, which contribute differences in therapeutic windows [10, 11]. Therefore, the role of Pyk2 in neonatal HI brain injury remains unclear. To evaluate the effects of Pyk2 in neonatal HI, we first assessed the activation of Pyk2 in hypoxic-ischemic brain injury in CD-1 mice pups. Then, to investigate the role of Pyk2 in neonatal HI, we constructed a Pyk2-interfering lentivirus and injected it before HI. The infarct volume, neurological behavior and the effects of Pyk2 were evaluated consecutively to assess the differences between the HI with Pyk2 inhibition group and the control group during the acute period. The recovery of cerebral blood flow, brain parenchymal volume and cognitive function were also tested to reveal long-term outcomes after neonatal HI brain injury with and without Pyk2. We report here that in the neonatal HI injury model, Pyk2 inhibition reduced brain damage and promoted behavioral recovery following hypoxic-ischemic injury. Our findings indicate that Pyk2 is a drug target for neonatal HI brain injury.

MATERIALS AND METHODS

Materials

Primary antibodies phospho-Pyk2 Y^{402} (Abcam, ab4800), Pyk2 (Abcam, ab226798), MAP2 (Abcam, ab11267), NeuN (Abcam, ab177487) and PSD95 (Abcam, ab12093) were purchased from Abcam (Cambridge, MA, USA). Primary antibody GluN1 (ABclonal, A7677), phospho-GluN1 S^{896} (ABclonal, AP0165), GluN2B (ABclonal, A3056), GluN2A (ABclonal, A13863), and phospho-GluN2B Y^{1474} (Abclonal, AP0771) were purchased from ABclonal Biotechnology Co., Ltd (Wuhan, China). GluN2A Y^{1325} (Bioss, bs-3305R) was purchased from Bioss Antibodies (Beijing, China). Primary antibodies phospho-AKT^{S473} (Cell Signaling Technology, 4051) and AKT (Cell Signaling Technology, 9272) were purchased from Cell Signaling Technology (Danvers, MA, USA). Primary antibody NOS2 (Santa Cruz Biotechnology, C-11, sc-7271 was purchased from Santa Cruz Biotechnology (Santa Cruz, CA, USA). Primary antibody β-actin (K200058M) and donkey serum (SL050) were purchased from Solarbio Life Sciences (Beijing, China). Alexa Fluor secondary antibodies (Invitrogen) were purchased from Thermo Fisher Scientific (Waltham, MA, USA). Horseradish peroxidase-coupled secondary antibodies were purchased from KPL (Gaithersburg, MD, USA).

TritonX-100 and MTT were purchased from Sigma-Aldrich (St. Louis, MO, USA). Cresyl violet, RIPA lysis buffer were purchased from Beyotime Biotechnology (Jiangsu, China). BCA kit was purchased from Applygen Technologies Inc. (Beijing, China). FD Rapid Golgi Stain Kit was purchased from FD Neurotechnology (Columbia, MD, USA). Dulbecco's modified Eagle's medium (DMEM) and reduced serum medium Opti-MEM were purchased from Gibco (Carlsbad, CA, USA). Polyvinylidene fluoride (PVDF) membranes were obtained from Millipore (Bedford, MA, USA). Prolong Antifade kit was purchased from Molecular Probes (Carlsbad, CA, USA). Membrane-permeable calcium ion fluorescent probe (40702ES50) was purchased from YEASEN Biotech Co. Ltd (Shanghai, China). Other materials were obtained from standard suppliers or as indicated in the text.

Animals

All animal care and experimental procedures complied with the principles outlined in the NIH Guide for the Care and Use of Laboratory Animals and were approved by the Institutional Animal Care and Use Committee of the Peking Union Medical College and Chinese Academy of Medical Sciences. The animal studies were performed in compliance with the ARRIVE guidelines and the Basel declaration, including the 3Rs concept [12, 13].

Pregnant CD-1 mice (gestational days 14–17) were purchased from SPF Biotechnology Co., Ltd. (Beijing, China). All animals were maintained in cages (one pregnant animal per cage) at a constant temperature and humidity under a 12:12 h light-dark cycle with unrestricted access to water and food except as indicated.

Animal experiments

The first set of experiments. CD-1 pups (postnatal day 7 (P7), either sex) were randomly divided into seven groups to evaluate the activation of Pyk2 at different time points after HI. The animals were anaesthetized with isoflurane and sacrificed by decapitation to obtain brain tissue for Western blotting for assessment of Pyk2 activation at different time points ($n = 5$ in each of the 7 groups).

The second set of experiments. CD-1 pups (P1) were divided into two groups to assess the efficiency of lentivirus infection by immunofluorescence ($n = 3$/group) and Western blotting ($n = 5$).

The third set of experiments. CD-1 pups (P1) were divided into three groups to study the effects of LV-Pyk2 short-hairpin RNA (shRNA). A diagram of the procedure is shown in Fig. 2b. Viral vectors were administered to P1 pups by intracerebroventricular (ICV) injection. HI was induced in P7 pups ($n = 18$/group). Twenty-four hours after HI, five pups from each group were anaesthetized with isoflurane and then decapitated to obtain brain tissue for TTC staining ($n = 5$/group) or perfused with 4% paraformaldehyde to obtain slices for TUNEL staining ($n = 3$). The remaining pups were subjected to behavioral assessments and MRI imaging ($n = 10$). Seven days after HI, half of the remaining experimental animals were anaesthetized with 3% isoflurane. The brains were fixed with 4% paraformaldehyde and then sliced for immunofluorescence and Nissl staining ($n = 5$/group). Tissues from the remaining animals were used for DNA and protein analysis.

The fourth set of experiments. CD-1 pups (P1) were divided into three viral vector groups. One hour after HI, P7 pups were anaesthetized with isoflurane and sacrificed by decapitation to obtain brain tissue for evaluation of NMDA activation using Western blotting ($n = 5$/group).

The fifth set of experiments. CD-1 pups (P1) were divided into three viral vector-treated groups for analysis of long-term recovery, including MRI, cerebral blood flow analysis, the MWM test, the novel object recognition test and Golgi staining ($n = 6$/group).

The sixth set of experiments. CD-1 pups (P1) were divided into three groups for analysis of long-term recovery following LV-HIF-Pyk2 shRNA-mediated inhibition, including the MWM test, the novel object recognition test and Golgi staining ($n = 5$/group).

The mortality rate was ~5%–11% depending on the HI model, intraventricular injection and the heterogeneity of the pups. Data for dead mice were excluded from the analysis. The list sample sizes (n) were the sizes after exclusion of dead mice and were used for analysis. Detailed data are shown in Table 1. Male and female pups were randomly selected for the experiments. All experiments were performed in a randomized and blinded manner. The experimental animals were deeply anaesthetized with 3% isoflurane before being decapitated or perfused.

Table 1. Detail of animal experiments.

Experiment	Total animal	Death/mortality	Animal for analysis
1st	37	2/5%	35
2nd	17	1/6%	16
3rd	59	5/8%	54
4th	17	2/11%	15
5th	20	2/10%	18
6th	17	2/11%	15

Lentivirus of Pyk2 inhibition
LV-Pyk2 shRNA, LV-HIF-Pyk2 shRNA and control vectors were constructed, packaged and concentrated by Obio Technology Corp., Ltd. (Shanghai, China).

LV-Pyk2 shRNA and LV-NC shRNA. A recombinant lentivirus was designed and produced to inhibit the expression of Ptk2b. Pyk2 shRNA (the target sequence: 5′-GCATAGAGTCAGACATCTA-3′) or control shRNA (the target sequence: 5′-TTCTCCGAACGTGT CACGT-3′) was inserted into the lentivirus vector pLKD-U6-shRNA-CMV-eGFP under the control of the U6 promoter, and eGFP was expressed under the control of the CMV promoter. The lentiviruses were named LV-Pyk2 shRNA and LV-NC shRNA.

LV-HIF-Pyk2 shRNA. The HIF-1α promoter was synthesized according to the vector pGL4.20-HIF-1α prom (Addgene #40173) and was inserted into the pLenti-CMV-EGFP-3FLAG-Micro30 shRNA (ptk2b) vector instead of the CMV promoter. The constructed lentivirus vector was pLenti-HIF-1α promoter-EGFP-3FLAG-micro30 shRNA (ptk2b) (a schematic is shown in Fig. 7a). The lentivirus was named LV-HIF-Pyk2 shRNA.

Injection of lentivirus into newborn mice
Intracerebroventricular (ICV) injection was performed according to a previously reported procedure [14]. Briefly, CD-1 pups (P1) were placed in a clean carton containing cotton from the home cage to maintain the mother's scent on a heating pad. The pups were anesthetized with 2% isoflurane before ICV injection, and anesthesia was maintained with 1.5% isoflurane. The injection was performed freehand using a 33G needle affixed to a 5 μL Hamilton syringe, and the pups received 3 μL LV-NC shRNA or LV-Pyk2 shRNA. Unilateral injections into the lateral ventricle were performed at 2/5 of the distance from the lambda suture to each eye and 3 mm deep. After the injection, the pups were allowed to recover on the heating pad for 10 min and then returned to their home cages.

Neonatal hypoxic-ischemic brain injury
An improved and modified hypoxic-ischemic brain injury model was used in this study [15–17]. P7 CD-1 pups of either sex were anesthetized with 2% isoflurane, and anesthesia was maintained with 1.5% isoflurane during the surgery. Body temperature was maintained using a heating pad. Using a standard sterile technique, the neck of each mouse pup was draped and prepared. After a small midline incision was made in the neck, the right common carotid artery was isolated from the surrounding structures, ligated twice with 5.0 surgical silk, and cut between the ligatures using electric coagulation forceps. The wound was closed with tissue adhesive, and anesthesia was stopped. The time for each surgery was maintained within 5 min, after which the pups were given 10 min to recover on the heating pad and then returned to their mothers for 60 min. After that, the pups were placed in an anoxic chamber and exposed to a mixture of 8% oxygen and 92% nitrogen for 60 min at 37 °C. The pups were returned to their home cages after hypoxic exposure.

TTC staining and infarct volume calculation
Twenty-four hours after HI, the pups were euthanized under anesthesia, and then their heads were removed and placed in a deep freezer at −80 °C for 2 min to freeze and harden the brains. The cold brains were removed from the skulls, and four coronal slices were cut (each slice was ~1 mm thick). The brain slices were then incubated in 1% (w/v) 2,3,5-triphenyltetrazolium chloride (TTC) solution at 37 °C for 15–20 min. The brain slices were then washed with PBS three times and kept in 10% paraformaldehyde solution at room temperature overnight. The infarcted and noninfarcted areas in each slice were outlined and measured with ImageJ software, and the damaged areas were then calculated. The infarct volume was calculated by multiplying the representative regions of all brain slices by the slice thickness. The infarction volume was calculated after correcting for edema as follows: corrected infarct volume (CIV), (%) = [contralateral hemisphere volume − (ipsilateral hemisphere volume − infarct volume)]/contralateral hemisphere volume × 100 [18].

Magnetic resonance imaging (MRI)
MRI scans were performed to assess the volume of edema. As previously described [19], the animals were anaesthetized with 1.5% isoflurane and fixed in a body restrainer with a tooth bar in an MRI spectrometer (Pharma Scan 70/16, Bruker, Germany). Their brains were scanned using a mouse head surface coil. T2-weighted images were acquired with the following parameters: repetition time of 5 min, matrix size of 256 × 256 pixels, field of view of 23 × 23 mm, acquisition time of 10 min, slice thickness of 0.3 mm, TR of 2800 ms, and TE_{eff} of 35 ms. For the recovery assay, 1 month later, whole brain coronal scans from the brain stem to the prefrontal cortex were obtained. The analyzed regions were the substantia nigra (−5.5 mm from bregma), hippocampus (−3 mm from bregma), striatum (0.5 mm from bregma), and prefrontal cortex (3 mm from bregma). The four regions analyzed were the same for newborn mice (P10) as for adult mice. Hyperintense infarct areas on T2-weighted images were assigned a region of interest and analyzed using Image-Pro Plus 6.0 software: infarct ratio (%) = total infarct area/total area × 100%.

Neurological behavioral tests
All neurobehavioral evaluations were performed in a blinded manner. Pups in each treatment group were subjected to multiple neurobehavioral tests 1, 3, and 7 days after HI. Each mouse was tested three times in each experiment, and each test lasted a maximum of 180 s.

Righting reflex. The righting reflex was assessed to study the combination of vestibular and somatosensory inputs for normal vertical positioning [15, 20]. Briefly, each pup was placed on its back on foam. The time needed for the pup to return to its feet was recorded.

Cliff avoidance reaction. Cliff avoidance was analyzed to evaluate maladaptive impulsive behavior [20, 21]. Each pup was placed on the edge of an elevated platform 15 cm high, which simulated a cliff environment, and both front paws were placed over the edge. The time needed for the pup to crawl away from the edge was recorded.

Geotaxis reflex. The geotaxis reflex was assessed to test vestibular and proprioceptive functions [20, 21]. The pups were placed with their heads downwards on a 45° slope. The time for the pups to turn ~90° toward the high end of the plane was recorded.

Grip test. The grip test was performed to assess grip force and fatigability [22]. The animals were suspended in both forepaws from a cotton rope (diameter, 1.5 mm) stretched horizontally 50 cm over a cotton pad. The time each mouse took to fall was recorded.

Cognitive recovery evaluation

The Morris water maze and novel object recognition tests were performed 4 weeks after HI to evaluate long-term recovery of neurological function.

Morris water maze. The Morris water maze test [23, 24] was performed to assess learning and memory ability. The mice were allowed to habituate at a water maze with a diameter of 1.1 m for 1 day and then tested. All the animals were subjected to both the cued and hidden tests, and the temperature of the water was maintained at 22 ± 1 °C. Each trial lasted for 60 s; if after 60 s, an animal could not find the platform, it was manually guided to it and allowed to stay on it for 10 s. The mice were trained twice per day over 5 consecutive days, with an intertrial interval of 4 h. The swimming activity of each mouse was monitored using a video camera (Sony, Tokyo, Japan) mounted over the maze and automatically recorded via a video tracking system. The escape latency (s) to reach the platform was recorded on the 5 training days. Approximately 24 h after the last learning trial, the mice were subjected to a probe trial without a platform. The number of target quadrant crossings and the total time spent in the target quadrant (s) were calculated to assess memory retention.

Novel object recognition. The novel object recognition test was performed according to a previously described method [25–27]. In the first trial, the mice were presented with two different objects placed in the upper two corners of a box (50 cm× 50 cm× 25 cm) for 5 min, and their activity was recorded. Then, the mice were removed from the box. Preference for a novel object was assessed on the subsequent day after a retention period of 24 h. The object on the right was replaced with a completely novel object in the same location. T_{new} (the time spent on exploring the new object) and T_{old} (the time spent on exploring the familiar object) were recorded. The discrimination index ($T_{new}/(T_{new} + T_{old})$) was used to evaluate investigation of the target object.

Long-term cerebral blood flow (CBF) measurement

The Full-Field Laser Perfusion Imager (FLPI2, Moor Instruments Ltd, UK) was used to image CBF to evaluate the recovery on the lesion side after HI [28]. The mice were exposed to 1.5% isoflurane inhalation via a facemask and placed in the prone position, and the skin was incised to access the skull. The surface was kept moist throughout the whole experiment. Blood flux was measured in a region of interest (ROI) that included most of the area affected by HI among different groups of animals, and the percentage of change in CBF was calculated with ImageJ software. The integrated optical density (IOD) of vessels or CBF within the ROI was calculated from blood vessel images (BV) or CBF images, respectively.

Primary neuron culture and lentivirus infection

Primary neurons were obtained from the cortices of fetal mice on the 14th day of gestation via a modified method [19, 29]. In short, the fetal mouse cortex was isolated by sterile manipulation. The tissue was dissociated into a single-cell suspension with 0.05% trypsin (Gibco, CA, USA) and then suspended in DMEM with 1% GlutaMAX I (Gibco, CA, USA) supplemented with 10% FBS (Gibco, CA, USA) and 1% penicillin-streptomycin (Gibco, CA, USA). After that, the cells were seeded in 24-well plates precoated with poly-*L*-lysine (PLL, Sigma, St. Louis, MO) at a density of 2×10^5 per well and cultured for 3 h to allow adherence (37 °C, 5% CO_2 in air). After that, the DMEM was replaced with neurobasal medium (97% neurobasal medium + 2% B27 + 1% GlutaMAX I), and half of the medium was replaced every 2 days. After 7 days of culture, the neurons were subjected to immunofluorescence with a MAP2 antibody, and the purity was determined. Primary neurons were cultured with the appropriate concentration of lentivirus (the titers of the lentiviruses were as follows: LV-NC shRNA: 6.55×10^8 TU/mL; LV-Pyk2 shRNA: 8.12×10^8 TU/mL; LV-HIF-Pyk2 shRNA: 1.78×10^9 TU/mL). The amount of virus added per well (μL) was calculated as the MOI × cell number/titer of lentivirus (TU/mL) × 1000. Primary hippocampal neurons were transfected at an MOI of 40. We added the appropriate amount of lentivirus according to the cell number. Lentiviral transfection and interference efficiency was measured by detection of GFP fluorescence and Western blot.

Cell oxygen-glucose deprivation (OGD) model

Primary neurons were subjected to OGD or transient oxygen-glucose deprivation/reoxygenation (OGD/R) according to previously described protocols [29]. Briefly, primary cortical neuronal cultures were incubated in D-Hanks medium at 37 °C in an anoxic chamber (95% N_2, 5% CO_2) for 1 h as OGD. Then, the neurons were cultured in neurobasal medium and placed in a normoxic environment (37 °C, 5% CO_2 in air) for 24 h as OGD/R.

Cell viability assay

The viability of primary neurons was quantified by the MTT assay (Sigma, CA, USA) [30]. Briefly, neurons were cultured in a 96-well plate at a density of 1×10^4 per well, with five replicate wells per group. The neurons were infected with LV-Pyk2 shRNA or control virus on the 7th day. The ODG/R model was established on the 10th day. Cell viability was determined by adding 25 μL of 5 mg·mL^{-1} MTT to each well on the 11th day. After 3 h of incubation at 37 °C, the medium was gently removed, and 150 μL DMSO was added. Finally, the number of viable cells was estimated by measuring the optical density (*OD*) at 570 nm using a multidetection microplate reader (Multiskan Go, Thermo, USA). The mean of five replicate wells per group was obtained. Cell viability was analyzed in five independent experiments. All the values were normalized to the mean of the control group and then multiplied by 100% to calculate cell viability.

Nissl staining

Coronal slices of the brains of mice subjected to HI were sectioned into 10 μm thick sections, dewaxed with xylene and 100% alcohol for 5 min each, and then stained with 0.5% cresyl violet (Beyotime, China) in a sealed wet box for 5 min at 37 °C. The excess cresyl violet was removed with PBS three times for 5 min. The sections were then quickly dehydrated in 100% ethanol for 10 s. Subsequently, the alcohol was removed by xylene before the sections were coverslipped. The slices were imaged using a light microscope (IX73, Olympus, Japan) and analyzed with ImageJ software.

TUNEL staining

TUNEL staining was used to identify and quantify apoptotic neuronal cells. Brain sections were collected 24 h after induction of HI stained using an In Situ Apoptosis Detection Kit (Roche, USA) according to the manufacturer's instructions [31]. Finally, the sections were covered with antifade mounting medium with DAPI (Beyotime, China). The slices were imaged using a fluorescence microscope (IX73, Olympus, Japan). The number of TUNEL-positive cells in each visual field was counted and determined with ImageJ software.

Immunofluorescence staining

Cells were grown on coverslips coated with PLL in 24-well plates, fixed in precooled acetone for 10 min, and washed three times for 5 min with PBS. The cells were permeabilized with 0.3% Triton X-100 for 15 min and blocked with 10% normal donkey serum for 1 h at room temperature. Then, the cells were incubated overnight at 4 °C with the following primary antibodies: rabbit anti-phospho-Pyk2 Y^{402} (1:200), mouse anti-MAP2 (1:1000), rabbit anti-NeuN (1:500), goat anti-PSD95 (1:500), rabbit anti-phospho-GluN1 S^{896} (1:100), and rabbit anti-phospho-GluN2B Y^{1474} (1:100, Y^{1474} in humans corresponds to Y^{1472} in rodents). The sections were

washed with PBS three times and then incubated with appropriate secondary antibodies (1:500) for 1 h at room temperature. The sections were then washed with 0.1% PBST three times for 5 min each. Finally, the sections were covered with antifade mounting medium with DAPI. The slides were then imaged under a Leica TSC SP8 CARS fluorescence microscope (Leica Microsystems, Germany) and analyzed using Leica Application Suite software and Huygens Professional software.

For staining of brain tissues, animals were anesthetized with isoflurane and then transcardially perfused with PBS followed by 4% formalin. The tissues were fixed overnight at 4 °C, dehydrated with gradient alcohol, embedded in paraffin, and then coronally sectioned into 10 μm thick slices. After deparaffinization, the slices were processed as mentioned above for immunofluorescence staining and imaging. Immunofluorescence staining in the cortices or hippocampus of five animals was quantified. Three sections per animal were included in the analyses.

Western blotting

Brains were prepared for Western blot analysis as previously described [32]. Briefly, animals were anesthetized with isoflurane, euthanized at different time points after HI, and then transcardially perfused with ice-cold PBS. The brains were removed, and ipsilateral brain tissues were isolated and stored immediately in a −80 °C freezer. Brain tissue samples were homogenized in RIPA lysis buffer for 30 min on ice and centrifuged at 13,000 × *g* at 4 °C for 30 min. The supernatants were collected, and the protein concentrations were assessed with a BCA kit. The proteins were separated on 4%–20% sodium dodecyl sulfate polyacrylamide gel electrophoresis gels and then transferred to PVDF membranes. After blocking with 5% BSA, the membranes were blotted with primary antibody at 4 °C overnight. The antibodies were as follows: anti-phospho-Pyk2 Y^{402} (1:1000), anti-t-Pyk2 (1:1000), anti-GluN1 (1:500), anti-GluN2B (1:500), anti-GluN2A (1:500), anti-phospho-GluN1 S^{896} (1:500), anti-phospho-GluN2B Y^{1474} (1:500 Y^{1472} in rodents), anti-phospho-GluN2A Y^{1325} (1:500), anti-phospho-AKT S^{473} (1:1000), anti-t-AKT (1:1000), anti-NOS2 (1:1000), and β-actin (1:1000). The membranes were incubated with secondary antibodies for 1 h at room temperature on the second day. The protein bands were visualized with an enhanced chemiluminescence (ECL) plus detection system (Molecular Device, Lmax). The density of each band was quantified using Gel-Pro Analyzer image analysis software (Media Cybernetics, MD, USA).

Golgi-Cox staining and dendritic spine counts

Golgi-Cox staining was employed to assess the morphology of synaptic spines [33]. A FD Rapid Golgi Stain Kit was used according to the manufacturer's instructions. In short, after the mice were sacrificed under anesthetization with isoflurane, the brain tissues were carefully removed as quickly as possible. The tissues were treated with impregnation solutions (A and B), which were replaced after 12 h, kept in total darkness, for two weeks and gently shaken once a week. Then, the brain tissues were transferred to solution C and kept in the dark for 3 days. The brains were cut into 50 μm thick sections on a freezing microtome (Leica, Germany), mounted on microscope slides with a drop of solution C, and then dried naturally in the dark. Finally, the slices were reacted in developing solution, dewaxed with 100% alcohol and xylene for 5 min each and covered with resinous mounting medium. Digital images were collected with a light microscope (IX73, Olympus, Japan), and the number of synaptic spines was measured with ImageJ software.

Calcium detection

A membrane-permeable calcium ion fluorescent probe (Lot: 40702ES50, YEASEN Biotech Co. Ltd, Shanghai, China) was used to detect calcium in neurons. HBSS was used to dilute the fluorescent probe to a concentration of 1 μM. The cultured primary neuron cells were incubated with the probe for 15 min and then washed three times with HBSS. The cells were subjected to OGD for 30 min. Fluorescence at 510 nm was detected by confocal microscopy.

Statistical analysis

All experiments were performed in a randomized and blinded manner. The sample size of each group was determined based on our previous similar studies. At least five samples per group ($n = 5$) were included in the statistical analysis, with n representing the number of independent values. The data are presented as the means ± SD. Statistical analyses were performed using GraphPad Prism 7. One-way ANOVA followed by the Newman–Keuls post hoc test was used for comparisons between multiple groups. Post hoc tests were performed only if F was significant and there was no variance in homogeneity. $P < 0.05$ was considered statistically significant.

RESULTS

Activation of Pyk2 in the neonatal brain after the HI

To check the status of Pyk2 after neonatal hypoxic-ischemic brain injury, HI was induced by unilateral common carotid artery ligation followed by hypoxic exposure (8% O_2, 1 h) in postnatal day 7 mouse pups. The time-course of the change in the level of p-Pyk2 Y^{402}, a marker of Pyk2 activation, was evaluated. The results showed that p-Pyk2 Y^{402} was highly expressed 0.5 h after HI injury. Then, upregulation of p-Pyk2 Y^{402} expression was maintained for at least 24 h (Fig. 1a, b), indicating its involvement in neonatal HI. Immunofluorescence of p-Pyk2 Y^{402} was also used to investigate its distribution after HI (Fig. 1c).

Pyk2 inhibition alleviates the neuronal damage induced by OGD in vitro

Activation of Pyk2 in response to neonatal HI might have some effect on neuronal damage. To confirm this speculation, we first linked the GFP reporter with Pyk2 shRNA or NC shRNA and packaged it as a lentivirus. Lentivirus infection and Pyk2 interference were assessed by GFP immunofluorescence and Western blotting, respectively (Fig. 1d, e). OGD was induced in primary mouse cortical neurons transfected with the above mentioned lentivirus. As shown in Fig. 1g, virally mediated Pyk2 inhibition attenuated neuronal cell damage caused by OGD. Neuronal cells were labeled with MAP2 to visualize their morphology and assess the degree of injury to neuronal cells after OGD. As shown in Fig. 1g, neuronal cell bodies were swollen and had fractured dendrites after OGD in the LV-NC shRNA-treated group, while the shape of neuronal cells was less affected in the LV-Pyk2 shRNA transfected group. The MTT assay results indicated that the cell viability of the LV-Pyk2 shRNA-treated group was also higher than that of the LV-NC shRNA-treated group after OGD/R (Fig. 1h). The in vitro test suggested that Pyk2 might mediate a harmful effect on neurons after anoxic injury.

Pyk2 inhibition attenuates acute brain injury after neonatal HI

To evaluate the in vivo effect of Pyk2 inhibition on HI, we injected Pyk2 shRNA or NC shRNA lentivirus into the right lateral ventricles of pups at P1. The in vivo effects of lentivirus infection were first assessed by measuring GFP expression, and then Pyk2 interference was compared using Western blot (Fig. 2a). We also performed the experiment as shown in the schematic to investigate whether Pyk2 inhibition could improve the general condition and neurobehavioral outcomes after HI (Fig. 2b). To compare HI brain damage in each group, TTC staining and histology were performed 24 h after neonatal HI. The cerebral infarction volume was significantly reduced in the LV-Pyk2 shRNA-treated group compared with the LV-NC shRNA-treated group

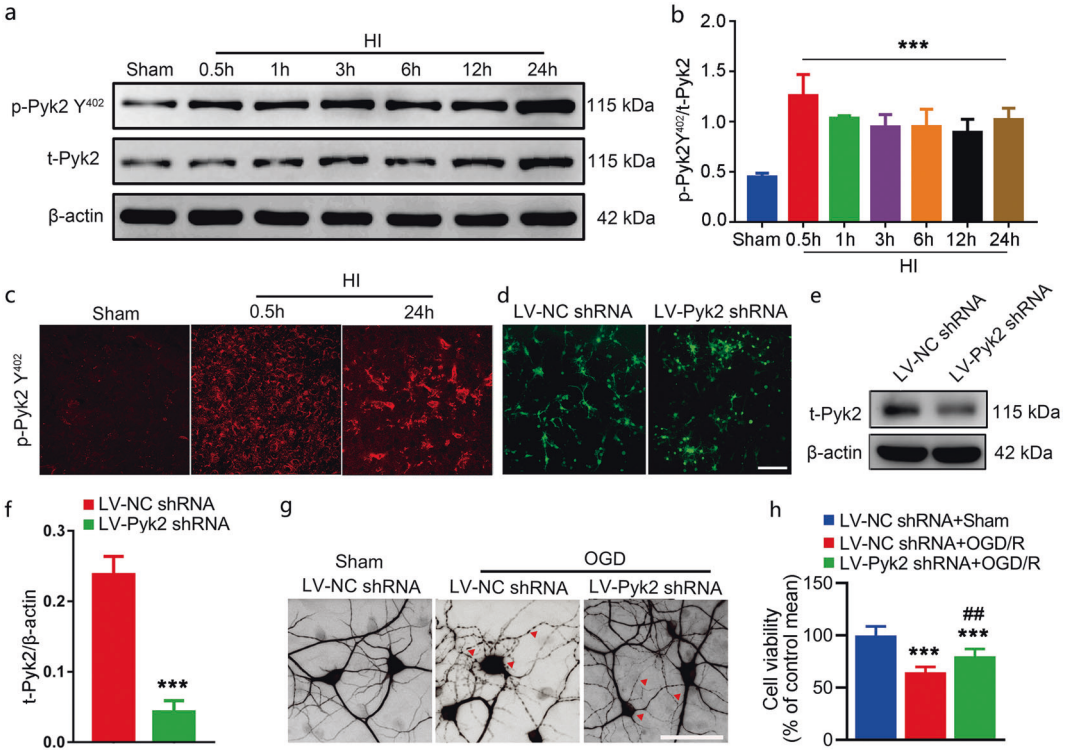

Fig. 1 Activation of Pyk2 after neonatal HI. a The phosphorylation of Pyk2 at Y^{402} was measured by Western blotting 0.5, 1, 3, 6, 12, and 24 h after HI brain injury. **b** The time-course of changes in the ratio of phosphorylated Pyk2 Y^{402} and Pyk2 Y^{402}. The data shown are means ± SD, $n = 5$ for each time point. $^{***}P < 0.001$ vs. the sham group. **c** Immunofluorescence staining of p-Pyk2 Y^{402} (red) in the cortex after HI. **d** Lentivirus infection of primary mouse cortical neurons was assessed by detecting GFP. **e**, **f** The inhibition of Pyk2 in neurons treated with viral vectors was evaluated by Western blotting. Pyk2 shRNA reduced total Pyk2 expression in Pyk2 shRNA-treated neurons. **g** The neuronal-specific marker MAP2 was used to identify primary mouse cortical neurons and assess their cytoskeleton morphology after OGD (bar = 5 μm). **h** Cell viability was assessed by the MTT assay after OGD/R. The data are presented as the means ± SD, $n = 5$. $^{***}P < 0.001$ vs. the LV-NC shRNA group in **f** and the LV-NC shRNA + sham group in **h**; $^{\#\#}P < 0.01$ vs. the LV-NC shRNA + OGD/R group.

after HI (Fig. 2c, d). MRI, which was performed on day 3 after HI, showed similar results as TTC staining (Fig. 2e, f). Survival of neuronal cells near the lesion area was assessed using NeuN, a marker of neuronal nuclei. The number of NeuN-positive cells in the ipsilateral cortex and hippocampus in the LV-Pyk2 shRNA-treated group was significantly greater than that in the LV-NC shRNA-treated group after HI, indicating less neuronal cell death in the Pyk2 inhibition group (Fig. 2g–i and Fig. S1). The TUNEL results revealed that the apoptosis of neurons in the ipsilateral hemisphere was also decreased in the LV-Pyk2 shRNA-treated group (Fig. 2j–l). Nissl staining was used to confirm the above results and showed that more cells survived in the Pyk2 inhibition group than in the control HI group (Fig. 2m–o).

Pyk2 inhibition improves the neurobehavioral outcomes of mice after neonatal HI

Body weight, seen as a general indicator of the recovery of pups, was measured on day 1, day 3, day 5, and day 7 after HI. From the results, we found that the Pyk2 inhibition group gained significantly more body weight than the control group beginning on the 5th day post HI, which might indicate a general improvement in condition (Fig. 3a). We assessed neurobehavioral performance to evaluate the effects of Pyk2 inhibition. The righting reflex was tested on day 1 and day 3 (Fig. 3b). The geotaxis reflex and cliff avoidance were evaluated on day 1, day 3 and day 7 after HI (Fig. 3c, d), and the grip test was performed at day 3 and day 7 after HI (Fig. 3e). In the righting reflex test and geotaxis reflex test, the Pyk2 inhibition group performed better than the control group beginning on the 1st day post HI, while performance on the cliff avoidance test was not different at that time point. The recovery of the forearm and all the above behavioral tests confirmed the improvement in the Pyk2 inhibition group compared with the LV-NC shRNA + HI group beginning on the 3rd day after HI. The in vivo behavioral test results were consistent with the in vivo brain damage results.

Pyk2 inhibition alleviates excitotoxic injury via NMDA receptors in neonatal HI

NMDA receptor activation is involved in acute neuronal damage after OGD. Pyk2 has been reported to bind PSD95 after ischemia [9, 34]. Thus, we first observed the colocalization of phosphorylated Pyk2 Y^{402} and PSD95 in cultured cortical neurons exposed to OGD. Colocalization increased significantly after OGD and was decreased in the LV-Pyk2 shRNA-treated neurons compared to the LV-NC shRNA-treated neurons (Fig. 4a, b and Fig. S2). Phosphorylation of Pyk2 has emerged as a fundamental mechanism that regulates NMDA receptor trafficking and can alter the channel properties of NMDA receptors [35]. Here, we evaluated the total and phosphorylated levels of several NMDAR subunits following inhibition of Pyk2. Immunofluorescence of phosphorylated GluN1 S^{896}, which is required for increasing the surface expression of NMDA receptors, was performed to evaluate the effect of Pyk2 inhibition on NMDA receptors after OGD (Fig. 4c, d). The phosphorylation of GluN2B subunits at Y^{1472}, the major phosphorylation site of NR2B, was also observed (Fig. 4e, f). Phosphorylation of GluN1 at S^{896} and GluN2B at Y^{1472} was found in the OGD group, which suggests enhanced NMDAR function with increased channel opening probability, calcium influx, and receptor recruitment to the membrane. In contrast, phosphorylation at these sites was lower in the LV-Pyk2 shRNA-treated group, which indicated a

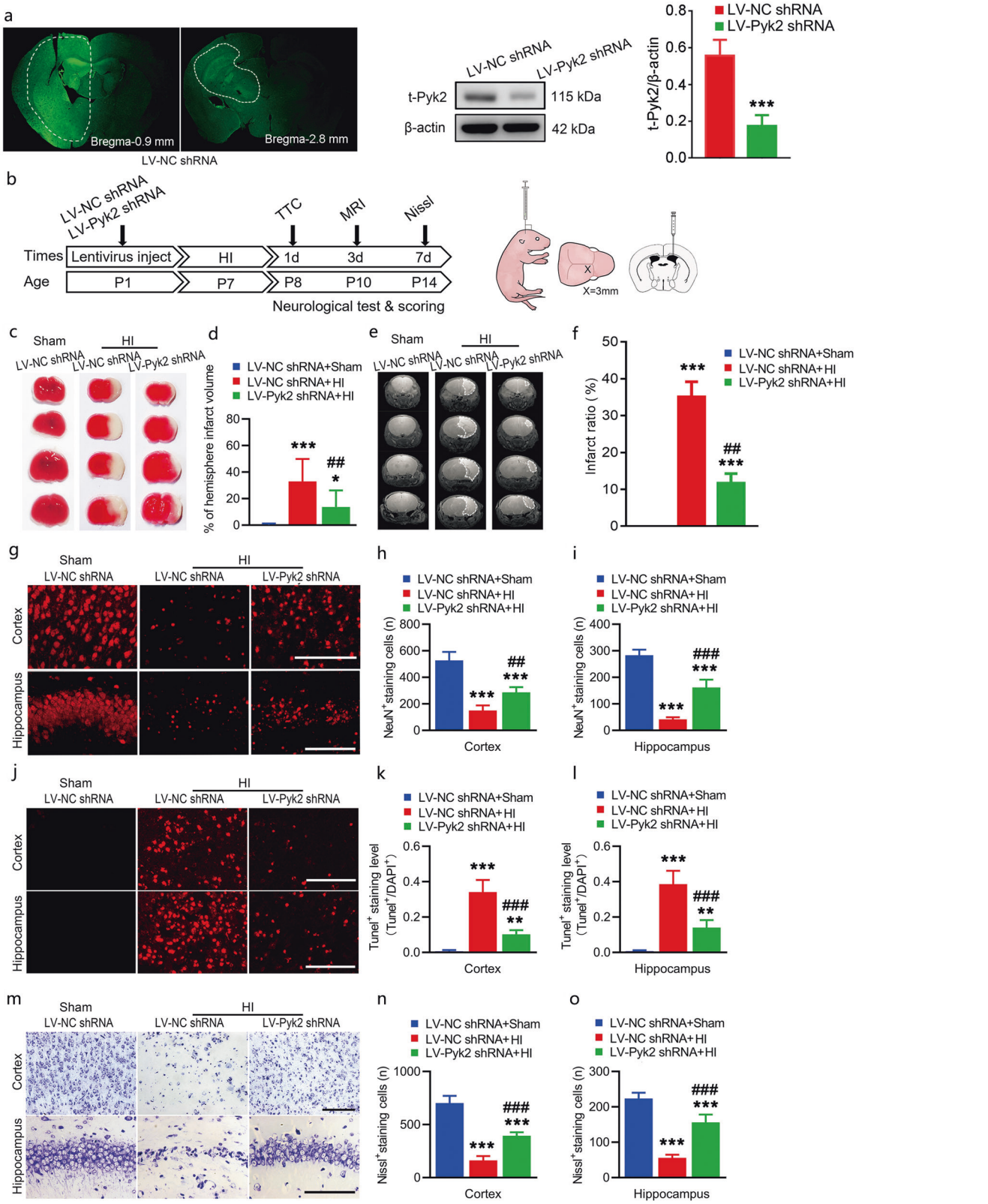

Fig. 2 Pyk2 inhibition alleviates acute brain injury after neonatal HI. a Lentivirus infection was assessed with detecting GFP expression in vivo. The inhibition of Pyk2 was evaluated by Western blotting in tissue from the transfected region in the LV-control shRNA- and LV-Pyk2 shRNA-treated groups ($n = 5$/group). **b** Schematic of the in vivo experimental procedure and the lentivirus-injected site. **c**, **d** TTC staining was used to determine the cerebral infarction volume after HI ($n = 5$/group). **e**, **f** MRI imaging showing the infarct ratio on day 3 after HI ($n = 10$/group). **g**–**i** The survival of neurons (NeuN labeled) in the ipsilateral cerebral cortices and hippocampi of mice after HI was assessed by immunofluorescence ($n = 5$/group; bar = 50 μm). **j**–**l** TUNEL-positive neurons in the ipsilateral cortices and hippocampi of mice were observed 24 h after HI ($n = 5$/group; bar = 50 μm). **m**–**o** Nissl staining of the ipsilateral cortices and hippocampi of mice after HI ($n = 5$/group; bar = 50 μm). The data are presented as the means ± SD. ***$P < 0.001$ vs. the LV-NC shRNA group in **a**; *$P < 0.05$, **$P < 0.01$, ***$P < 0.001$ vs. the LV-NC shRNA + sham group in **d**, **f**, **h**, **i**, **k**, **l**, **n**, and **o**; ##$P < 0.01$ and ###$P < 0.001$ vs. the LV-NC shRNA + HI group.

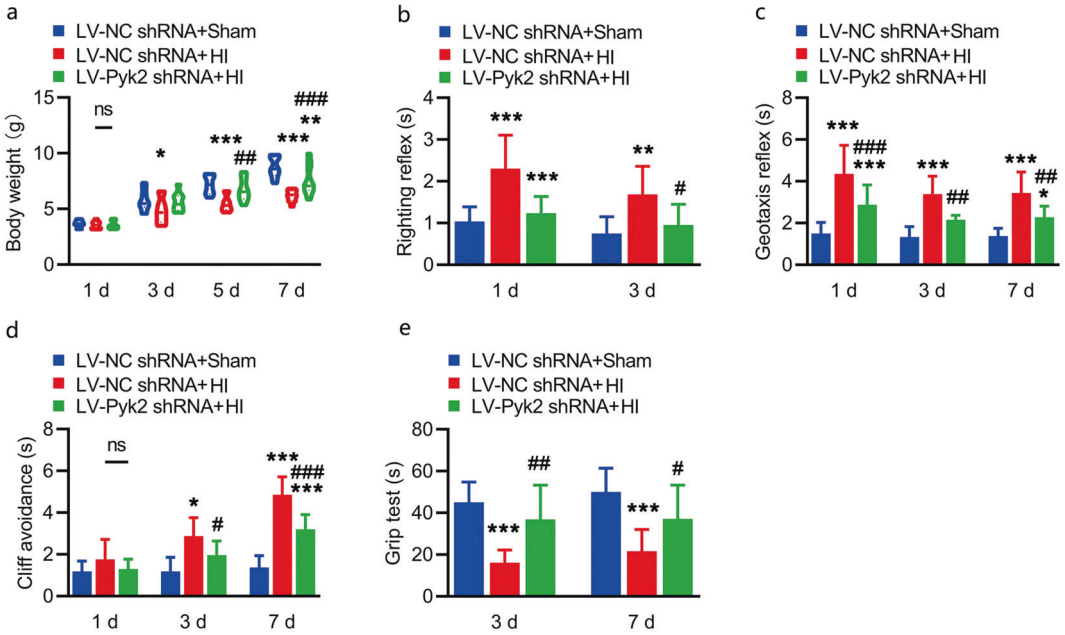

Fig. 3 Pyk2 inhibition improves the general condition and neurobehavioral outcomes after HI. a Body weight was measured after HI and compared between the different groups. **b** The righting reflex was assessed on day 1 and day 3 after HI. **c** The geotaxis reflex ability was tested on day 1, day 3, and day 7 after HI. **d** Cliff avoidance was tested on day 1, day 3, and day 7 after HI. **e** The grip test was performed on day 3 and day 7 after HI. The data are presented as the means ± SD, $n = 10$. $^{*}P < 0.05$, $^{**}P < 0.01$, and $^{***}P < 0.001$ vs. the LV-NC shRNA + sham group; $^{\#}P < 0.05$, $^{\#\#}P < 0.01$, and $^{\#\#\#}P < 0.001$ vs. the LV-NC shRNA + HI group.

reduction in excitatory neurotoxicity caused by OGD (Fig. 4e, f). We also tested Ca^{2+} influx in primary hippocampal neurons in our experiment using a membrane-permeable calcium ion fluorescent probe (Fig. 4g). The probe spots suggested that the overload of Ca^{2+} in neurons after OGD treatment was associated with cellular swelling, which was alleviated by the inhibition of Pyk2. A calcium colorimetric assay also confirmed this result (Fig. 4h).

As we speculated that an increase in the levels of postsynaptic density scaffolds might mediate the activation of NMDA receptors, we evaluated the levels of total and phosphorylated protein for several NMDA receptors that participate in the activation of excitotoxicity 0.5 h after HI by Western blot analysis. The total levels of the NMDA receptors GluN1, GluN2A and GluN2B were not significantly changed in mice treated with LV-Pyk2 shRNA compared with those treated with LV-NC shRNA (Fig. 5a, b). The p-GluN1 S^{896} and p-GluN2A Y^{1472} levels after HI were significantly increased in the LV-NC shRNA-treated group and were decreased in the LV-Pyk2 shRNA-treated group, while the level of p-GluN2A Y^{1325} was not obviously changed with or without the inhibition of Pyk2 (Fig. 5c, d). As shown by the above results, NMDA receptors were highly activated after HI, while these changes were prevented by Pyk2 inhibition, revealing the role of Pyk2 in excitotoxicity in vivo. To further test our hypothesis, we also measured the levels of NOS2 and phosphorylated AKT, the key proteins of the NMDA signaling pathway [15]. Inhibition of Pyk2 significantly reduced the level of NOS2 and the increase in p-AKT S^{473} expression after HI (Fig. 5e–g). Collectively, these findings suggest that Pyk2 inhibition might prevent overactivation of NMDA receptors (p-GluN1 S^{896} and p-GluN2A Y^{1472}) and thus reduce neurotoxic injury.

Pyk2 inhibition contributes to the long-term recovery of the cerebrovascular unit but limited cognitive recovery after neonatal HI

To determine the long-term effect of Pyk2 inhibition on HI brain injury, we employed MRI to assess the recovery of mice 4 weeks after HI. The MRI results confirmed that inhibition of Pyk2 contributed to alleviation of brain injury after HI (Fig. 6a, b). Blood vessel density (Fig. 6c, d) and cerebral blood flow (Fig. 6c, e) were also preserved in the LV-Pyk2 shRNA-treated group compared with the LV-NC shRNA-treated group after HI. Next, we evaluated the long-term effect of Pyk2 inhibition on cognition after HI. For long-term cognitive function assessment, the Morris water maze test was used. The results showed that the LV-Pyk2 shRNA-treated group performed better than the LV-NC shRNA-treated group in the probe trial 4 weeks after HI (Fig. 6f–h). We were not able to find any difference in performance in the novel object recognition test between the LV-Pyk2 shRNA- and LV-NC shRNA-treated groups 4 weeks after HI (Fig. 6i). To determine why, Golgi-Cox staining was used to label synaptic spines in the ipsilateral hemisphere. Fine structures of axons, such as axonal spines, are normally damaged and reduced in number after ischemia and/or hypoxia. In our study, inhibition of Pyk2 only resulted in an increasing trend in the number of spines in the LV-Pyk2 shRNA group after neonatal HI (Fig. 6j, k). However, inhibition of Pyk2 following neonatal HI alleviated brain damage but was not able to rescue and preserve most synaptic spines, as determined by ultrastructural analysis of the brain. Thus, it may limit some of the behavioral outcomes after HI.

Hypoxia-induced Pyk2 inhibition improves cognitive dysfunction after neonatal HI

According to the above mentioned results, long-term Pyk2 inhibition might hinder synaptic recovery and thus affect cognition. We constructed a new vector that inhibited Pyk2 under the control of the HIF-1α promoter (Fig. 7a). To check the validity of the HIF-1α promoter, we transfected primary cortical culture neurons in vitro using the constructed lentivirus. GFP was inserted as the indicator. The results showed that the HIF promoter was activated after OGD and inactivated after reperfusion (OGD/R), which demonstrated that Pyk2 interference was controlled by hypoxia (Fig. 7b). Long-term cognitive recovery was tested again to evaluate the effect of hypoxia-induced Pyk2 inhibition initiated under hypoxic conditions. Mice treated with LV-HIF-Pyk2 shRNA found the hidden platform more quickly and spent more time in the target quadrant in the probe trial of the Morris water maze test than mice treated with LV-Pyk2 shRNA or LV-NC shRNA (Fig. 7c–e).

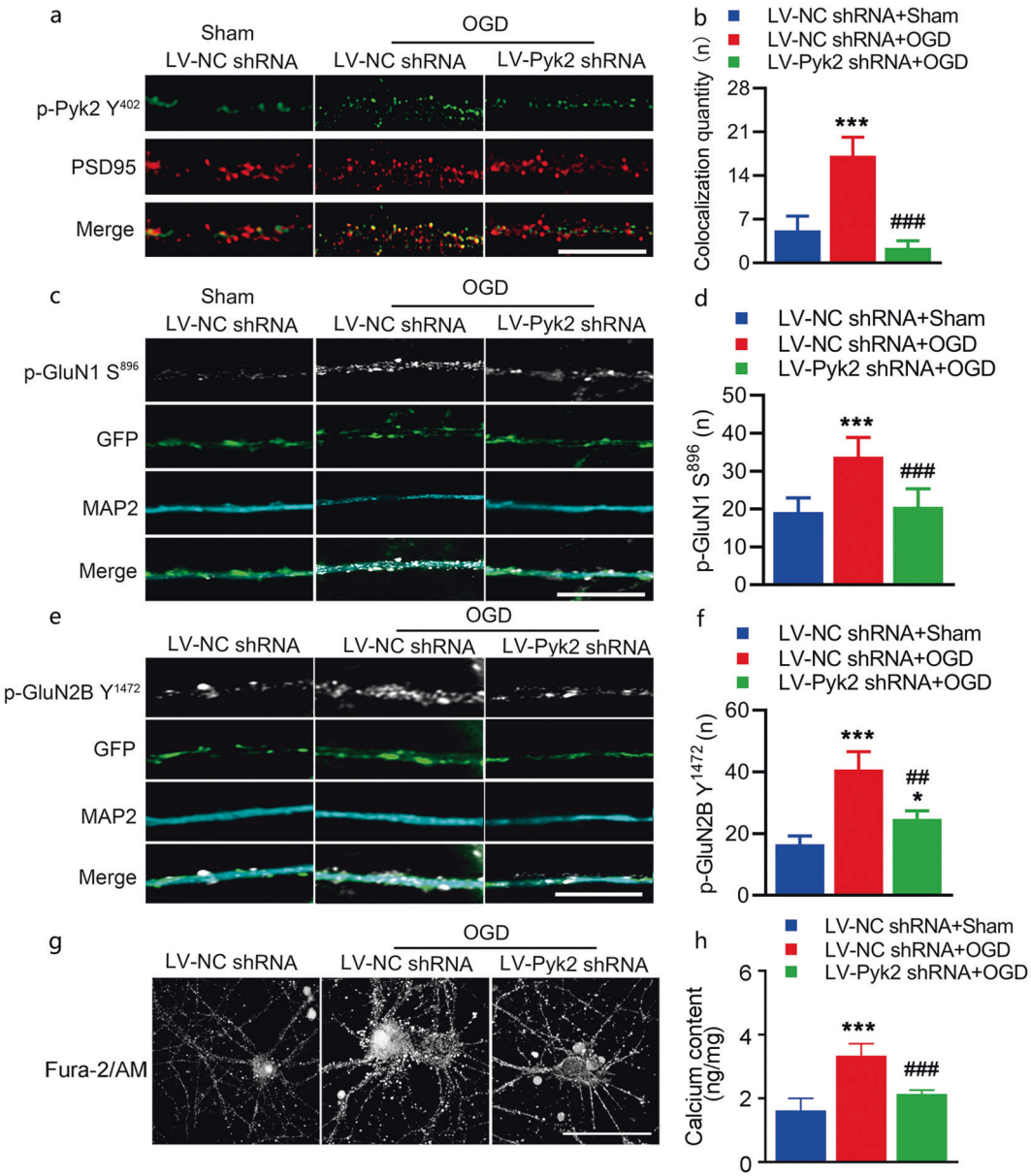

Fig. 4 Pyk2 inhibition reduces NMDA receptor-mediated neurotoxic injury in vitro. a, **b** Cultured cortical neurons were double stained with PSD95 and p-Pyk2 Y^{402} antibodies after OGD (bar = 10 μm). The colocalization of PSD95 and p-Pyk2 Y^{402} was quantified by counting yellow spots on axons with a length of 15 μm. Four axons from each group were included in each experiment. Data from five independent experiments were included in the analyses. p-Pyk2 Y^{402} was pseudocolored green. **c**, **d** Representative immunofluorescence images of NMDA receptor p-GluN1 S^{896} in the dendrites of cultured cortical neurons. The number of p-GluN1 S^{896}-positive spots was increased after OGD; LV-Pyk2 shRNA pretreatment suppressed the increase in p-GluN1 S^{896} level after OGD (bar = 10 μm). **e**, **f** Representative immunofluorescence images of the NMDA receptor p-GluN2B Y^{1472} in the dendrites of cultured cortical neurons (bar = 10 μm). **g** A membrane-permeable calcium ion fluorescent probe was used to detect Ca^{2+} in neurons (bar = 5 μm). **h** A calcium colorimetric assay was performed. The data are presented as the means ± SD, $n = 5$/group. ***$P < 0.001$ vs. the LV-NC shRNA + sham group; $^{\#\#}P < 0.01$ and $^{\#\#\#}P < 0.001$ vs. the LV-NC shRNA + OGD group.

The LV-HIF-Pyk2 treated group also showed improved cognition in the novel object recognition test (Fig. 7f). In addition, the density of synaptic spines in the LV-HIF-Pyk2 treated group was significantly increased, indicating the preservation of physiological functions and support for some behavioral functions (Fig. 7g, h).

DISCUSSION

Neonatal HI brain injury and related brain disorders cause long-term disability. Approximately one-quarter of HIE survivors exhibit permanent neuropsychological disability similar to cerebral palsy with or without learning and intellectual disabilities as well as epilepsy. These individuals need lifelong care. There is no effective pharmaceutical intervention to ameliorate brain damage or improve neurological function in HIE infants except for limited clinical ventilation and mild hypothermia. Many interventions have targeted NMDA receptor-mediated excitotoxicity to treat acute ischemic brain injury and stroke in adults for decades without success thus far. Owing to the dual function of NMDA receptors and the side effects of potential drugs for stroke that block NMDARs, focus has shifted to PSD95, a scaffolding protein, which is involved in clustering glutamate receptors together with

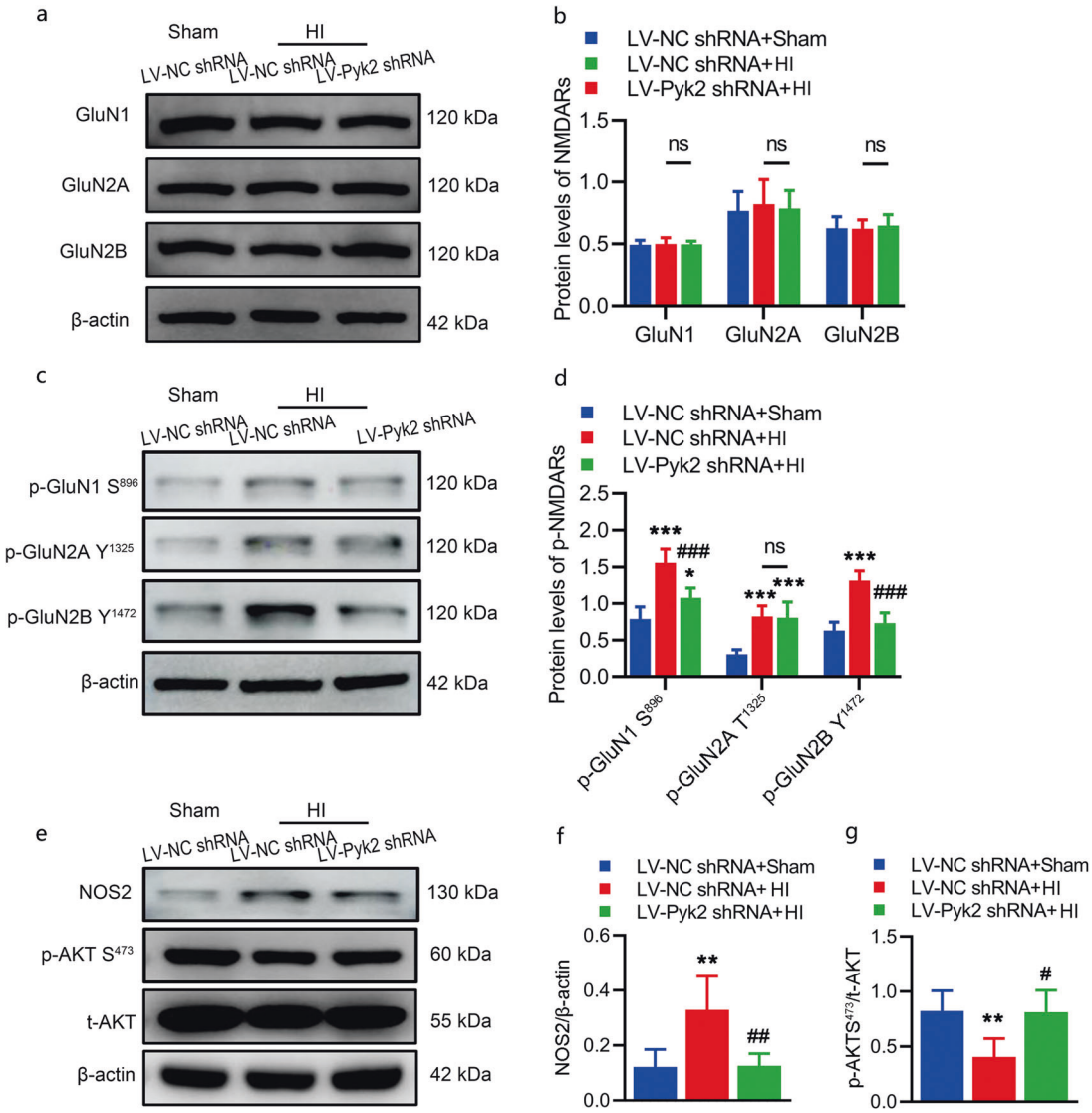

Fig. 5 Pyk2 inhibition alleviates excitotoxic injury via NMDA receptors following neonatal HI. a, **b** WB analysis of the expression of NMDA receptor proteins, including GluN1, GluN2A, and GluN2B, in the ipsilateral hemisphere after HI. **c**, **d** WB analysis of the phosphorylation NMDA receptor subunits, i.e., phosphorylation of GluN1 at S^{896}, GluN2A at Y^{1325} and GluN2B at Y^{1472} after HI. **e**–**g** WB analysis of the expression of NOS2 and p-AKT S^{473} in the ipsilateral hemisphere after HI. The data are presented as the means ± SD, $n = 5$/group. $^{*}P < 0.05$, $^{**}P < 0.01$, and $^{***}P < 0.001$ vs. the LV-NC shRNA + sham group; $^{\#}P < 0.05$, $^{\#\#}P < 0.01$, and $^{\#\#\#}P < 0.001$ vs. the LV-NC shRNA + HI group.

other proteins at postsynaptic sites such as neuronal nitric-oxide synthetase, Ras-activating SynGAP, and calcium/calmodulin-dependent protein kinase II [6, 36, 37]. Pyk2 has been demonstrated to mediate the interaction of the NMDA receptor complex mediated by PSD-95 [38]. It has been reported the *I/R* increases the activation of Pyk2 as well as the interaction between Pyk2 and NR2A, which promotes the influx of Ca^{2+} through NMDA receptors and promotes NMDA receptor function in adults [39, 40]. However, neonatal HI brain injury is not the same as adult I/R, mainly due to differences in metabolism and NMDA receptor expression between adult and neonatal brains, which contribute differences in therapeutic windows [3, 4]. The development-related alteration in the ratio of NR2A:NR2B is reflected by differences in receptor properties, which indicate differences in the sensitivity of neonatal animals to HI-induced neuronal cell damage [5]. Therefore, the effect and therapeutic window of Pyk2 interference in the neonatal brain after HI are still largely unknown. Furthermore, according to previous research, Pyk2 has been suppressed either concomitantly with other treatments, such as under lithium [9], or by intraventricular injection of antisense oligonucleotides for several days before four-vessel occlusion. The results of these studies lack specificity and feasibility for neonatal hypoxia-ischemia due to the administration route or model [41]. In this study, the role and mechanism of Pyk2 in neonatal HI brain injury were studied in P7 CD-1 mouse pups. Brain development in animals of this age is similar to that in near-term human babies [42, 43]. In this study, we investigated whether Pyk2 participates in neonatal hypoxic-ischemic brain injury and whether Pyk2 inhibition alleviates HI brain injury. We report here for the first time that Pyk2 is activated after HI (Fig. 1). Pyk2 inhibition significantly reduced neonatal HI brain damage and improved neurobehavioral outcomes in a mouse neonatal hypoxic-ischemic brain injury model (Fig. 2 and 3).

In adults, transient brain ischemia followed by reperfusion enhances the autophosphorylation of Pyk2 at Tyr-402. Pyk2 interacts with PSD-95 through multiple residues [38]. I/R can also increase the interactions between p-Pyk2 and NR2A as well as between Pyk2 and PSD95. In our study, neonatal HI resulted in activation of Pyk2, which colocalized with PSD95. Phosphorylation of GluN1 at S^{896} is required to increase the surface expression of

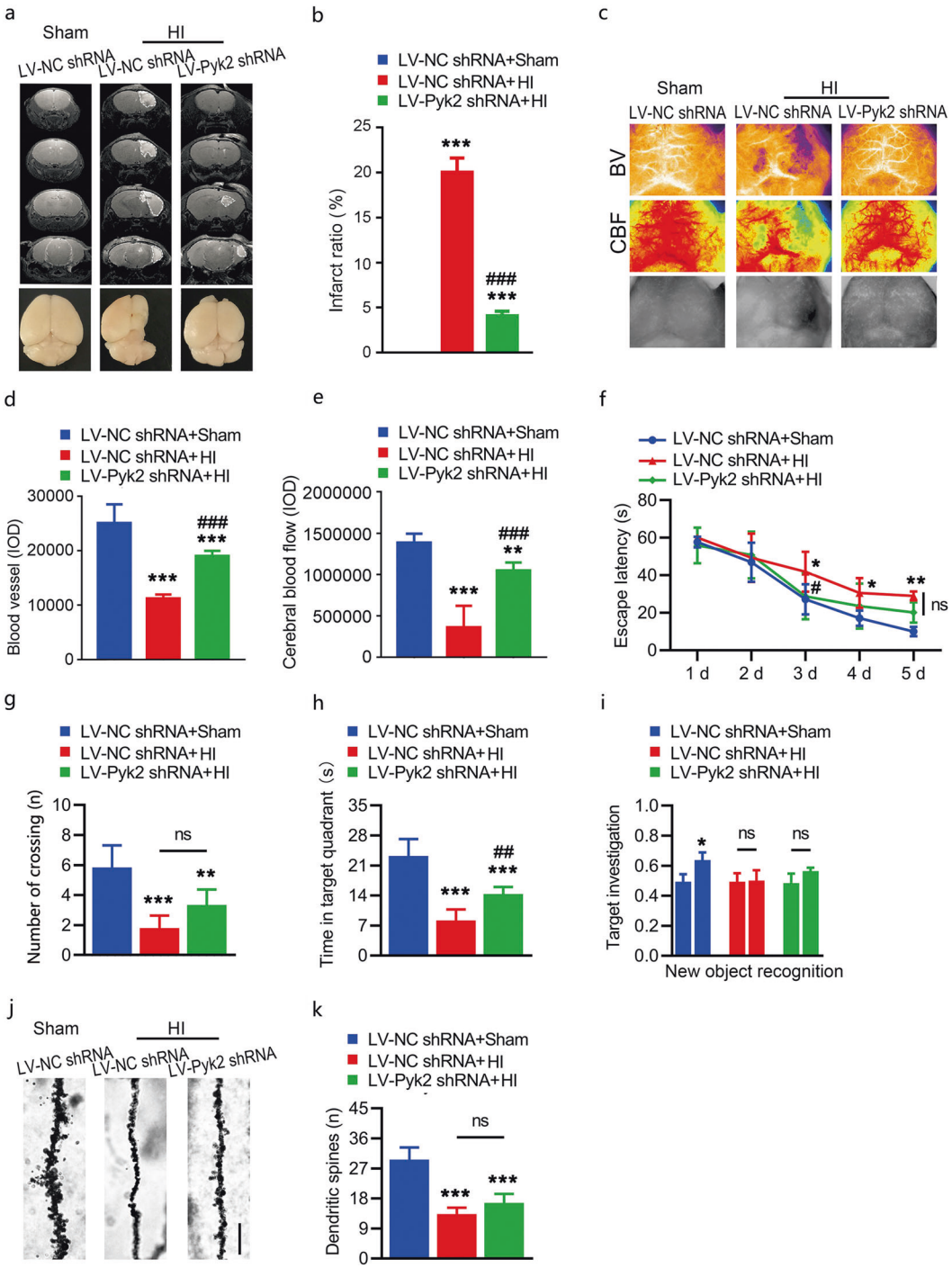

Fig. 6 Effect of Pyk2 inhibition on long-term recovery after HI. a, **b** Representative MRI images of each group 4 weeks after HI. Lower panels are whole-brain images showing brain the shapes of the different groups. **c**–**e** A full-field laser perfusion imager was used to assess long-term cerebral blood flow (CBF) and blood vessel recovery. **f**–**h** The Morris water maze test was performed 4 weeks after HI. **i** The discrimination index was calculated to evaluate investigation of the novel object in the novel object recognition test. **j**–**k** Golgi-Cox impregnation showing the morphology of synaptic spines in the ipsilateral hemisphere in different groups after HI (bar = 3 μm). The data are presented as the means ± SD, $n = 6$/group. *$P < 0.05$, **$P < 0.01$, and ***$P < 0.001$ vs. the LV-NC shRNA + sham group; $^{\#\#}P < 0.01$ and $^{\#\#\#}P < 0.001$ vs. the LV-NC shRNA + HI group.

NMDA receptors [44]. Y^{1472} is the major tyrosine phosphorylation site in NR2B. Phosphorylation of Y^{1472} in NR2B stabilizes NMDA receptors on the plasma membrane, which is important for brain physiology. A sustained increase in Y^{1472} phosphorylation initiates downstream cell death signaling and thus contributes to brain injury [45]. In our study, the phosphorylation of GluN1 at S^{896} and GluN2B at Y^{1472} was tested in vivo and in vitro (Fig. 4 and 5). The model group showed the enhancement of phosphorylation at these sites, which was consistent with the enhanced NMDAR function, indicating increased calcium influx, as shown in Fig. 4g, h. Pyk2 inhibition significantly reduced the phosphorylation of GluN1 at S^{896} and GluN2B at Y^{1472}. As a tyrosine kinase, Pyk2 cannot be directly responsible for the phosphorylation of GluN1 at S^{896}; thus, these changes indicate a role for Pyk2 in hypoxic-ischemic

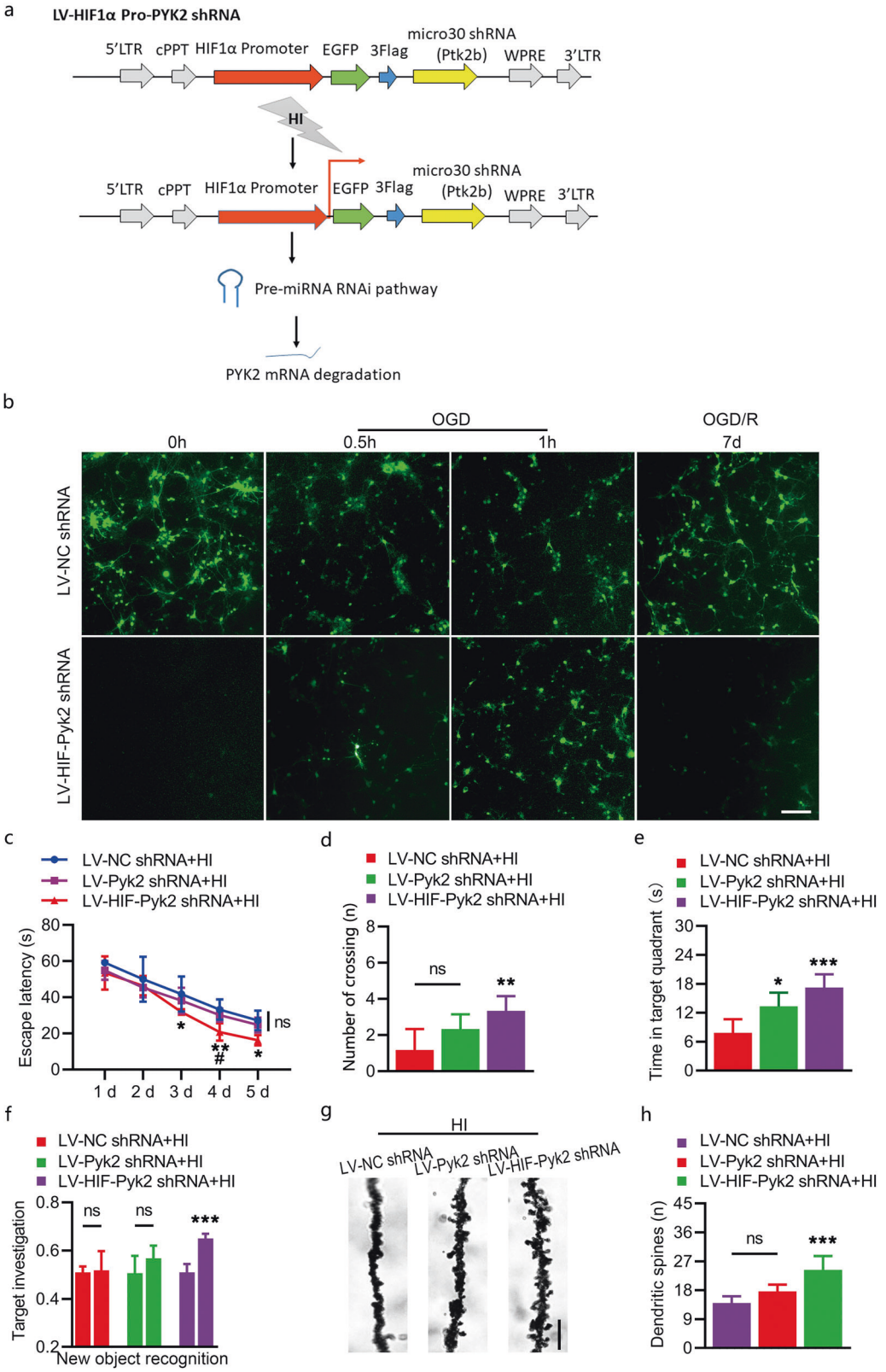

Fig. 7 Effect of hypoxia-induced Pyk2 inhibition on cognitive function recovery after HI. a Schematic of LV-HIF-Pyk2, which was used for hypoxia-induced Pyk2 inhibition. **b** Primary cortical culture neurons transfected with different lentiviruses showed different GFP expression patterns during OGD and OGD/R. Imaging of GFP fluorescence showed that the HIF promoter was activated after OGD and inactivated after reperfusion (OGD/R). **c**–**e** Long-term neurocognitive function was evaluated using the Morris water maze test. **f** Neurocognitive function was tested using the novel object recognition test. **g**–**h** Golgi-Cox impregnation imaging showed the density of synaptic spines four weeks after HI (bar = 3 μm). The data are presented as the means ± SD, $n = 5$/group. $^{*}P < 0.05$, $^{**}P < 0.01$, and $^{***}P < 0.001$ vs. the LV-NC shRNA + HI group; $^{\#}P < 0.05$ vs. the LV-Pyk2 shRNA + HI group.

processes after HI, which is at least in part due to its interaction with PSD95. In addition, Pyk2 inhibition did not affect the activation of the NMDA receptor p-GluN2A Y^{1325}, which confirmed the specificity of Pyk2 in neonatal HI (Fig. 5c, d).

Regarding the duration of the phosphorylation and interaction of Pyk2, it has been reported that in adults, although the interaction between phospho-Pyk2 and NR2A is reduced to normal levels 24 h after reperfusion, the enhancement of the interaction between Pyk2 and PSD95 through other residues of Pyk2 persists [9]. Additionally, our results showed persistent activation of Pyk2 following neonatal HI. Although the phosphorylation of glutamate receptors was only assessed early after injury, the levels of downstream proteins were changed (Fig. 5e), and damage to the ultrastructure of dendrites was also shown (Fig. 1g). Twenty-four hours after HI, neuronal cell death and brain damage already occurred; our results showed that Pyk2 inhibition alleviated acute neonatal HI brain injury (Fig. 2j). Neonatal HI brain injury has unique features due to immaturity of the neonatal nervous system, which causes apoptosis and necrosis to co-occur in the injured neonatal brain [46].

In addition to the interaction between Pyk2 and NMDAR discussed in our study, there might be other mechanisms related to the complex role of Pyk2 in neonatal HI, such as its function in brain–immune interactions after HI. HI provokes an intravascular inflammatory cascade that is further amplified by the activation of resident immune cells and the cerebral infiltration of peripheral immune cells. This prolonged inappropriate neuroinflammation leads to secondary injury of brain tissue [47]. Since the activation of Pyk2 persists and is maintained 24 h after HI, it may also participate in the recruitment of immune cells. We also assessed the colocalization of p-Pyk2 Y^{402} with Iba-1 (a marker of microglia) and GFAP (a marker of astrocytes) after neonatal HI (data not shown). We found that p-Pyk2 Y^{402} was also expressed in microglia and played a role in microglial polarization. These mechanisms are currently being studied.

No significant differences between male and female pups were noticed in our preliminary experiment, which is also consistent with research by Jaworska and co-workers [15, 48]; thus, male and female pups were randomly selected for the experiment. However, some researchers suggest that there are sex differences that can be observed after perinatal brain injury [49, 50]. We will give full consideration to sex differences in our next study.

HI causes more damage to the neonatal brain because it is a development period. We evaluated the recovery of cerebral blood flow and brain volume in the experimental animals 30 days after HI. Considering the neuroprotective effect of Pyk2 inhibition, the cerebral blood flow, vascular abundance and brain volume in mice in the Pyk2 intervention group were significantly improved after HI (Fig. 6a–e). However, according to some cognitive tests, the effect of Pyk2 inhibition was limited. Pyk2 is considered to play an important role in spine structure and synaptic function [33], although Salazar et al. reported that the absence of Pyk2 has no major effect on synapse formation or basal parameters of synaptic transmission in the hippocampal Schaffer collateral pathway [51]. As shown by our Golgi staining results, Pyk2 intervention did not result in spine recovery despite aiding restoration of cerebral blood flow and vasculature (Fig. 6j, k), which may indicate that Pyk2 has an effect on fine synaptic structures. We speculate that this is because of the difference in age of the experimental animals. Our mice were ~1-month-old during the testing period after HI, and Pyk2 may not be compensated by other homologs, such as FAK, during the period of neuronal development. Therefore, synaptic structure was shown to be affected by the inhibition of Pyk2. To confirm this speculation, we constructed a virally packaged vector containing the HIF-1α promoter that induced Pyk2 inhibition only during HI and then assessed long-term cognitive effects after HI. Pyk2 intervention was restricted to pathological conditions by the HIF-1α promoter (Fig. 7a). When mediated by an anoxic environment, Pyk2 inhibition improved cognition after HI.

The aim of this study was to determine the role of Pyk2 as a target for future drug development. Whether inhibition of Pyk2 could be beneficial for neonatal HI and the timing of the effect are both currently unknown. The use of antagonists and genetic manipulation are two recognized strategies. Both require intraventricular injection. However, there are three main limitations to the use of Pyk2 antagonists. First, all Pyk2 antagonists discovered to date nonspecific, as they are FAK/Pyk2 antagonists, such as PF431396 and BI-4464. They are ~10 times more selective for FAK than Pyk2. Second, intraventricular injection after HI is not a good impact on evaluation, considering the time needed for recovery after injection and neonatal vulnerability. Third, the appropriate timing of the administration of the antagonist needs to be determined and verified, especially during the first few hours of damage. In addition to those identified in this study, Pyk2 might also work through other mechanisms after HI due to its cellular localization and time-dependent expression; therefore, we performed genetic manipulation almost one week before HI to allow full expression of the element expressed by the vector and recovery from intraventricular injection to exclude the influences of the procedure. We observed the overall effect of Pyk2 inhibition on the treatment of neonatal HI, which was the purpose of this experimental stage. After confirming the results, we will focus on the interactions, time of onset and mode of administration and blood-brain barrier penetrates.

In conclusion, there is still no effective treatment for neonatal hypoxic-ischemic brain injury. This study demonstrates that Pyk2 inhibition attenuates damage due to neonatal HI injury during the acute and recovery periods. The HIF-1α promoter can mediate inhibition of targets according to changes in the cellular environment. These findings deepen our understanding of the immature brain and may have significant implications for therapies for neonatal hypoxic-ischemic brain injury and related hypoxic-ischemic encephalopathy. Our current study suggests that Pyk2 is a potential drug target for neonatal HI brain injury.

ACKNOWLEDGEMENTS

This work was supported by the National Natural Science Foundation of China (81730096, 81873026, 81973499), the CAMS Innovation Fund for Medical Sciences (CIFMS) (2016-I2M-1-004), the Drug Innovation Major Project (2018ZX09711001-003-005, 2018ZX09711001-002-007), the Beijing Key Laboratory of New Drug Mechanisms and Pharmacological Evaluation Study (BZ0150), the opening Program of Shanxi Key Laboratory of Chinese Medicine Encephalopathy (CME-OP-2017001), and the High-End Foreign Experts introduction program (G20200001485).

AUTHOR CONTRIBUTIONS

NHC and ZZ designed research. JZ performed the animal models and all the cell and WB experiments; YP, DDL, and WXJ assisted the experiment, ZZ and CC analyze the data; SFC reviewed the data; JZ and ZZ drafted the manuscript; HSS and ZPF guided the animal experiments; HSS, ZPF, and NHC revised the manuscript.

ADDITIONAL INFORMATION

Supplementary information The online version contains supplementary material available at https://doi.org/10.1038/s41401-021-00694-5.

Competing interests: The authors declare no competing interests.

REFERENCES

1. Higgins RD. Hypoxic ischemic encephalopathy and hypothermia: a critical look. Obstet Gynecol. 2005;106:1385–7.
2. Douglas-Escobar M, Weiss MD. Hypoxic-ischemic encephalopathy: a review for the clinician. JAMA Pediatr. 2015;169:397–403.
3. Kurinczuk JJ, White-Koning M, Badawi N. Epidemiology of neonatal encephalopathy and hypoxic-ischaemic encephalopathy. Early Hum Dev. 2010;86:329–38.

4. Dixon BJ, Reis C, Ho WM, Tang J, Zhang JH. Neuroprotective strategies after neonatal hypoxic ischemic encephalopathy. Int J Mol Sci. 2015;16:22368–401.
5. Pregnolato S, Chakkarapani E, Isles AR, Luyt K. Glutamate transport and preterm brain injury. Front Physiol. 2019;10:417.
6. Davis SM, Lees KR, Albers GW, Diener HC, Markabi S, Karlsson G, et al. Selfotel in acute ischemic stroke: possible neurotoxic effects of an NMDA antagonist. Stroke. 2000;31:347–54.
7. Ikonomidou C, Bosch F, Miksa M, Bittigau P, Vockler J, Dikranian K, et al. Blockade of NMDA receptors and apoptotic neurodegeneration in the developing brain. Science. 1999;283:70–4.
8. Tian D, Litvak V, Lev S. Cerebral ischemia and seizures induce tyrosine phosphorylation of PYK2 in neurons and microglial cells. J Neurosci. 2000;20:6478–87.
9. Ma J, Zhang GY, Liu Y, Yan JZ, Hao ZB. Lithium suppressed Tyr-402 phosphorylation of proline-rich tyrosine kinase (Pyk2) and interactions of Pyk2 and PSD-95 with NR2A in rat hippocampus following cerebral ischemia. Neurosci Res. 2004;49:357–62.
10. Wenzel A, Fritschy JM, Mohler H, Benke D. NMDA receptor heterogeneity during postnatal development of the rat brain: differential expression of the NR2A, NR2B, and NR2C subunit proteins. J Neurochem. 1997;68:469–78.
11. Sans N, Petralia RS, Wang YX, Blahos J 2nd, Hell JW, Wenthold RJ. A developmental change in NMDA receptor-associated proteins at hippocampal synapses. J Neurosci. 2000;20:1260–71.
12. Kilkenny C, Browne W, Cuthill IC, Emerson M, Altman DG, Group NCRRGW. Animal research: reporting in vivo experiments: the ARRIVE guidelines. Br J Pharmacol. 2010;160:1577–9.
13. McGrath JC, Lilley E. Implementing guidelines on reporting research using animals (ARRIVE etc.): new requirements for publication in BJP. Br J Pharmacol. 2015;172:3189–93.
14. Hasselmann J, Coburn MA, England W, Figueroa Velez DX, Kiani Shabestari S, Tu CH, et al. Development of a chimeric model to study and manipulate human microglia in vivo. Neuron. 2019;103:1016–33.
15. Xu B, Xiao AJ, Chen W, Turlova E, Liu R, Barszczyk A, et al. Neuroprotective effects of a PSD-95 inhibitor in neonatal hypoxic-ischemic brain injury. Mol Neurobiol. 2016;53:5962–70.
16. Rice JE 3rd, Vannucci RC, Brierley JB. The influence of immaturity on hypoxic-ischemic brain damage in the rat. Ann Neurol. 1981;9:131–41.
17. Levine S. Anoxic-ischemic encephalopathy in rats. Am J Pathol. 1960;36:1–17.
18. Qi X, Hosoi T, Okuma Y, Kaneko M, Nomura Y. Sodium 4-phenylbutyrate protects against cerebral ischemic injury. Mol Pharmacol. 2004;66:899–908.
19. Chen C, Chu SF, Ai QD, Zhang Z, Guan FF, Wang SS, et al. CKLF1 aggravates focal cerebral ischemia injury at early stage partly by modulating microglia/macrophage toward m1 polarization through CCR4. Cell Mol Neurobiol. 2019;39:651–69.
20. Sun HS, Xu B, Chen W, Xiao A, Turlova E, Alibraham A, et al. Neuronal K(ATP) channels mediate hypoxic preconditioning and reduce subsequent neonatal hypoxic-ischemic brain injury. Exp Neurol. 2015;263:161–71.
21. Chen W, Xu B, Xiao A, Liu L, Fang X, Liu R, et al. TRPM7 inhibitor carvacrol protects brain from neonatal hypoxic-ischemic injury. Mol Brain. 2015;8:11.
22. Liu XH, Yan H, Xu M, Zhao YL, Li LM, Zhou XH, et al. Hyperbaric oxygenation reduces long-term brain injury and ameliorates behavioral function by suppression of apoptosis in a rat model of neonatal hypoxia-ischemia. Neurochem Int. 2013;62:922–30.
23. Morris R. Developments of a water-maze procedure for studying spatial learning in the rat. J Neurosci Methods. 1984;11:47–60.
24. Sun HS, Jackson MF, Martin LJ, Jansen K, Teves L, Cui H, et al. Suppression of hippocampal TRPM7 protein prevents delayed neuronal death in brain ischemia. Nat Neurosci. 2009;12:1300–7.
25. Huang YR, Xie XX, Ji M, Yu XL, Zhu J, Zhang LX, et al. Naturally occurring autoantibodies against alpha-synuclein rescues memory and motor deficits and attenuates alpha-synuclein pathology in mouse model of Parkinson's disease. Neurobiol Dis. 2019;124:202–17.
26. Liu SY, Lu S, Yu XL, Yang SG, Liu W, Liu XM, et al. Fruitless wolfberry-sprout extract rescued cognitive deficits and attenuated neuropathology in Alzheimer's disease transgenic mice. Curr Alzheimer Res. 2018;15:856–68.
27. Zhang Z, Chu SF, Wang SS, Jiang YN, Gao Y, Yang PF, et al. RTP801 is a critical factor in the neurodegeneration process of A53T alpha-synuclein in a mouse model of Parkinson's disease under chronic restraint stress. Br J Pharmacol. 2018;175:590–605.
28. Kang N, Zhang J, Yu X, Ma Y. Radial extracorporeal shock wave therapy improves cerebral blood flow and neurological function in a rat model of cerebral ischemia. Am J Transl Res. 2017;9:2000–12.
29. Chu SF, Zhang Z, Zhou X, He WB, Chen C, Luo P, et al. Ginsenoside Rg1 protects against ischemic/reperfusion-induced neuronal injury through miR-144/Nrf2/ARE pathway. Acta Pharmacol Sin. 2019;40:13–25.
30. Sun XY, Dong QX, Zhu J, Sun X, Zhang LF, Qiu M, et al. Resveratrol rescues tau-induced cognitive deficits and neuropathology in a mouse model of tauopathy. Curr Alzheimer Res. 2019;16:710–22.
31. Liu SY, Yu XL, Zhu J, Liu XM, Zhang Y, Dong QX, et al. Intravenous immunoglobulin ameliorates motor and cognitive deficits and neuropathology in R6/2 mouse model of Huntington's disease by decreasing mutant huntingtin protein level and normalizing NF-kappaB signaling pathway. Brain Res. 2018;1697:21–33.
32. Zha J, Liu XM, Zhu J, Liu SY, Lu S, Xu PX, et al. A scFv antibody targeting common oligomeric epitope has potential for treating several amyloidoses. Sci Rep-Uk. 2016;6:36631.
33. Giralt A, Brito V, Chevy Q, Simonnet C, Otsu Y, Cifuentes-Diaz C, et al. Pyk2 modulates hippocampal excitatory synapses and contributes to cognitive deficits in a Huntington's disease model. Nat Commun. 2017;8:15592.
34. Besshoh S, Bawa D, Teves L, Wallace MC, Gurd JW. Increased phosphorylation and redistribution of NMDA receptors between synaptic lipid rafts and post-synaptic densities following transient global ischemia in the rat brain. J Neurochem. 2005;93:186–94.
35. Montalban E, Al-Massadi O, Sancho-Balsells A, Brito V, de Pins B, Alberch J, et al. Pyk2 in the amygdala modulates chronic stress sequelae via PSD-95-related micro-structural changes. Transl Psychiatry. 2019;9:3.
36. Aarts M, Liu Y, Liu L, Besshoh S, Arundine M, Gurd JW, et al. Treatment of ischemic brain damage by perturbing NMDA receptor-PSD-95 protein interactions. Science. 2002;298:846–50.
37. Sun HS, Doucette TA, Liu Y, Fang Y, Teves L, Aarts M, et al. Effectiveness of PSD95 inhibitors in permanent and transient focal ischemia in the rat. Stroke. 2008;39:2544–53.
38. Seabold GK, Burette A, Lim IA, Weinberg RJ, Hell JW. Interaction of the tyrosine kinase Pyk2 with the N-methyl-D-aspartate receptor complex via the Src homology 3 domains of PSD-95 and SAP102. J Biol Chem. 2003;278:15040–8.
39. Liu Y, Zhang GY, Hou XY, Xu TL. Two types of calcium channels regulating activation of proline-rich tyrosine kinase 2 induced by transient brain ischemia in rat hippocampus. Neurosci Lett. 2003;348:127–30.
40. Liu Y, Zhang G, Gao C, Hou X. NMDA receptor activation results in tyrosine phosphorylation of NMDA receptor subunit 2A(NR2A) and interaction of Pyk2 and Src with NR2A after transient cerebral ischemia and reperfusion. Brain Res. 2001;909:51–8.
41. Liu Y, Zhang GY, Yan JZ, Xu TL. Suppression of Pyk2 attenuated the increased tyrosine phosphorylation of NMDA receptor subunit 2A after brain ischemia in rat hippocampus. Neurosci Lett. 2005;379:55–8.
42. Clancy B, Darlington RB, Finlay BL. Translating developmental time across mammalian species. Neuroscience. 2001;105:7–17.
43. Rumajogee P, Bregman T, Miller SP, Yager JY, Fehlings MG. Rodent hypoxia-ischemia models for cerebral palsy research: a systematic review. Front Neurol. 2016;7:57.
44. Scott DB, Blanpied TA, Swanson GT, Zhang C, Ehlers MD. An NMDA receptor ER retention signal regulated by phosphorylation and alternative splicing. J Neurosci. 2001;21:3063–72.
45. Knox R, Brennan-Minnella AM, Lu F, Yang D, Nakazawa T, Yamamoto T, et al. NR2B phosphorylation at tyrosine 1472 contributes to brain injury in a rodent model of neonatal hypoxia-ischemia. Stroke. 2014;45:3040–7.
46. Northington FJ, Zelaya ME, O'Riordan DP, Blomgren K, Flock DL, Hagberg H, et al. Failure to complete apoptosis following neonatal hypoxia-ischemia manifests as "continuum" phenotype of cell death and occurs with multiple manifestations of mitochondrial dysfunction in rodent forebrain. Neuroscience. 2007;149:822–33.
47. Li B, Concepcion K, Meng X, Zhang L. Brain-immune interactions in perinatal hypoxic-ischemic brain injury. Prog Neurobiol. 2017;159:50–68.
48. Ziemka-Nalecz M, Jaworska J, Sypecka J, Polowy R, Filipkowski RK, Zalewska T. Sodium butyrate, a histone deacetylase inhibitor, exhibits neuroprotective/neurogenic effects in a rat model of neonatal hypoxia-ischemia. Mol Neurobiol. 2017;54:5300–18.
49. Hurn PD, Vannucci SJ, Hagberg H. Adult or perinatal brain injury: does sex matter? Stroke. 2005;36:193–5.
50. Johnston MV, Hagberg H. Sex and the pathogenesis of cerebral palsy. Dev Med Child Neurol. 2007;49:74–8.
51. Salazar SV, Cox TO, Lee S, Brody AH, Chyung AS, Haas LT, et al. Alzheimer's disease risk factor Pyk2 mediates amyloid-beta-induced synaptic dysfunction and loss. J Neurosci. 2019;39:758–72.